National Oceanographic Partnership Program 2011 Broad Agency Announcement, Funding Opportunity Number NOAA-NOS-IOOS-2011-2002515, CFDA Number: 11.012, Integrated Ocean Observing System (IOOS) Topic Area 3, "Improved and Routine Production, Stewardship, and Application of the Group for High Resolution Sea Surface Temperature (GHRSST) Data."

Final Progress Report for
November 15, 2012 through November 14, 2017

Multi-sensor Improved Sea Surface Temperature (MISST) for (IOOS)

NASA Contract No. NNH13CH09C

Principal- Investigator: Chelle L. Gentemann, Earth and Space Research

Partners: Peter J. Minnett, University of Miami
Andy Harris, University of Maryland
Erik Crosman, University of Utah
Carl Mears, Remote Sensing Systems

Final summary:

Collaborations and coordinations

- Coordination with IOOS RAs and inclusion of MISST SST products for their user base.
- Improved SSTs available at IOOS websites, new data products created to address specific IOOS requests, improvements to SSTs, and RA's access to new high resolution SSTs.
- Participation in annual GHRSST science team meetings and coordination of US with international research plans.

IR SSTs

- Improvements to data availability and IR SST accuracy through new algorithm formulations, improved calibrations and better removal of cloud contaminated data. Terra MODIS, Aqua MODIS, VIIRS, MSG, and MTSAT.
- Analysis of cloud-induced sampling errors in temporally averaged Terra MODIS SSTs can be reduced by sampling an SST anomaly field, relative to a daily climatology. The magnitudes and characteristics of sampling errors were found to be largely independent of the reference SST field used in the assessment, whether it be satellite-based or a modelled field.
- Analysis of sampling errors in MODIS SSTs global fields has been extended to VIIRS. A second paper on the MODIS sampling errors has been published in *Remote Sensing of Environment*. Application of new cloud and error masking and SST retrieval to MODIS data has been published. Inclusion of aerosol in state vector for physical retrieval shown to improve both algorithm accuracy and sensitivity to SST. Validation results may now be limited by the accuracy of *in situ* data.

- Evidence has been uncovered through analysis of the VIIRS match-up data base of a "response vs scan angle effect." This is presumably occurring at the half-angle mirror. An empirical correction has been developed and is being further investigated.
- Reprocessing of geostationary SST data back to September 2002 using MTLS physical retrieval algorithm.

PMW SSTs

- Re-processing, updating, NRT data production and distribution of MW OI, MWIR OI, AMSR2, AMSRE, TMI, and GMI in GDS 2.0.
- Validation papers for AMSR-E and AMSR2 SSTs completed and published.

In situ

- In collaboration with Scripps Institution of Oceanography, a study has begun to assess how well drifting buoy thermometers retain their calibration after deployment by mooring a cluster of buoys off the RSMAS pier for several years, and recovering them periodically to check their calibration.

Lake SSTs

- Validation of NASA MUR SST analyses and NOAA Coastwatch SST over inland lakes were conducted. *In situ* data was used from the Great Salt Lake, Lake Okeechobee, Lake Oneida, and Lake Michigan for the period 2007-2015. Significant cloud contamination and temporal compositing errors identified. A collaborative paper with NASA JPL on satellite-derived lake temperature entitled "Evaluation of the Multi-Scale Ultra-High Resolution (MUR) Analysis of Lake Surface Temperature" was published in a special SST issue of *Remote Sensing* (13 July 2017). http://www.mdpi.com/2072-4292/9/7/723.
- An extensive review of lake SST's (over 300 references) is nearing completion and is expected to be submitted to *Remote Sensing of Environment* by the end of December 2017. A major goal of this paper to provide guidance for future directions and improvements needed in the validation of, algorithms used, and availability of satellite-derived lake temperature for both numerical weather prediction and climate studies.
- A paper was published in the *Journal of Atmospheric and Oceanic Technology* that provided methodologies for improved cloud contamination and improved statistical methods for spatial and temporal lake SST analyses for numerical weather prediction.
- Coordination with NOAA/NWS/NASA for testing MUR lake SST climatology as first guess field for potential use in NOAA/NWS operational RTG lake products over North American lakes for a wide range of lake sizes ranging from 10 km- 100's km.

M-AERI

- M-AERIs have been reinstalled on *Celebrity Equinox* and *Allure of the Seas* after refurbishment and recalibration at RSMAS. A third M-AERI has been readied for installation on the *Adventure of the Seas* in early 2018; similarly the fourth M-AERI is ready to be deployed on the NOAA Ship *Ronald H Brown* also in early 2018.
- An M-AERI and the RSMAS water-bath blackbody calibration target were part of an international workshop at the National Physical Laboratory (NPL) in the UK. The instruments were referenced to SI standards at the NPL. The workshop was conducted under the auspices of the Committee for Earth Observation Satellites (CEOS) and it's Working Group on Calibration and Validation (WGCV). Two papers are in preparation for publication in the reviewed literature.

Diurnal Warming

- Two publications on diurnal warming modeling (satellite observed compared to Zeng-Beljaars modeled) have been submitted to *Journal of Geophys. Res. Oceans.*
- A study of diurnal heating in the Mediterranean Sea and its consequences on the heat and freshwater budget has been completed and a paper published in the *Journal of Geophysical Research*.

Papers published/submitted:

1. Minnett, P.J., Kilpatrick, K., Podestá, G., Szczodrak, M., Izaguirre, M.A., Williams, E., Walsh, S., Evans, R.H., & Reynolds, R.M. (2018). Suomi-NPP VIIRS Sea Surface Temperature retrievals; algorithm evolution and an assessment of uncertainties. *Remote Sensing of Environment*. In review.
2. Ditri, A.L., Minnett, P.J., Liu, Y., Kilpatrick, K., & Kumar, A. (2018). The Accuracies of Himawari-8 and MTSAT-2 Sea-Surface Temperatures in the Tropical Western Pacific Ocean. *Remote Sensing.* In review.
3. Zhu, X., P. J. Minnett, H. Beggs and R. Berkelmans (2018). Thermal features and diurnal warming at the Great Barrier Reef derived from satellite data, submitted to *Remote Sensing of Environment.* In revision.
4. Gentemann, C.L. and S. Akella, Evaluation of NASA GEOS-ADAS modeled diurnal warming through comparisons 1 to SEVIRI and AMSR2 SST observations, *in revision J. Geophys. Res. Oceans.*
5. Wong, E. W. and P. J. Minnett (2018). The response of the ocean thermal skin layer to variations in incident infrared radiation, *submitted J. Geophys. Res. Oceans.* In revision.
6. Zhang, H., H. Beggs, X. H. Wang, J. Rodriguez, L. Thorpe, M. A. Brunke, L. Majewski, A. E. Kiss, and C. L. Gentemann, Comparison of SST Diurnal Variation Models over the Tropical Warm Pool*, submitted J. Geophys. Res. Oceans.*
7. Zhu, X., E. Maturi, A. Harris, J. Mittaz, P. Koner, M. Eakin, R. Potash, A reprocessed record of geostationary sea surface temperatures using physical retrieval and Bayesian cloud detection, submitted to *Rem. Sens. Environ.*, 2017.
8. Liu, Y., T.M. Chin, and P. J. Minnett (2017), Sampling errors in satellite-derived infrared sea-surface temperatures. Part II: Sensitivity and parameterization. *Remote Sensing of Environment*, 198, 297-309. *http://dx.doi.org/10.1016/j.rse.2017.06.011*
9. Crosman, E.T., J. Vazquez, and T.M. Chin (2017), Evaluation of the Multi-scale Ultra-high Resolution (MUR) Analysis of Lake Surface Temperature, *Remote Sensing, 9(7),* 723*; doi:10.3390/rs9070723*
10. Maturi, E., A. Harris, J. Mittaz, J. Sapper, G. Wick, X. Zhu, P. Dash, and P. Koner (2017), A New High-Resolution Sea Surface Temperature Blended Analysis, Bulletin of the American Meteorological Society, 98(5), 1015-1026, doi:10.1175/bams-d-15-00002.1.
11. Gentemann, C. L., M. R. Fewings, and M. García-Reyes (2017), Satellite sea surface temperatures along the West Coast of the United States during the 2014–2016 northeast Pacific marine heat wave, *Geophys. Res. Lett.*, 43, doi:10.1002/2016GL071039.
12. Koner, P., Harris, A.R., and Maturi, E.M., (2016) Hybrid cloud and error masking to improve the quality of deterministic satellite sea surface temperature retrieval and data coverage, *Rem. Sens. Environ.*, **174**, 266-278.

13. Wong, E., & Minnett, P.J. (2016). Retrieval of the ocean skin temperature profiles from measurements of infrared hyperspectral radiometers. Part I: Evaluation of the truncated singular value decomposition technique. *IEEE Transactions on Geoscience and Remote Sensing*. 54, 1879-1890.
14. Wong, E., & Minnett, P.J. (2016). Retrieval of the ocean skin temperature profiles from measurements of infrared hyperspectral radiometers. Part II: Field data analysis. *IEEE Transactions on Geoscience and Remote Sensing*. 54, 1891-1904.
15. Liu, Y., & Minnett, P.J. (2016). Global sampling errors and error variability of MODIS Sea-Surface Temperatures. *Remote Sensing of Environment*. 177, 48-64
16. Koner, P. K., A. Harris, and E. Maturi (2016), Hybrid cloud and error masking to improve the quality of deterministic satellite sea surface temperature retrieval and data coverage, Remote Sensing of Environment, 174(Supplement C), 266-278, doi:https://doi.org/10.1016/j.rse.2015.12.015.
17. Koner, P., and Harris, A.R., (2016). Improved quality of MODIS sea surface temperature retrieval and data coverage using physical deterministic methods. *Remote Sensing*. **8**(6), 454; doi:10.3390/rs8060454.
18. Koner, P., and Harris, A.R., (2016). Sea surface temperature retrieval from MODIS radiances using truncated total least squares with multiple channels and parameters. *Remote Sensing*, **8**, 725; doi:10.3390/rs8090725
19. Marullo, S., P. J. Minnett, R. Santoleri, and M. Tonani (2016), The Diurnal Cycle of Sea-Surface Temperature and Estimation of the Heat Budget of the Mediterranean Sea, *Journal of Geophysical Research*, 121.11: 8351-8367.
20. Gentemann, C.L. and K.A. Hilburn, (2015) "In situ validation of sea surface temperatures from the GCOM-W1 AMSR2 RSS calibrated brightness temperature", *J. Geophy. Res*., 120*(5*), 3567-3585.
21. Liu, Y., and P.J. Minnett. (2015) Evidence Linking Satellite-derived Sea-Surface Temperature Signals to Changes in the Atlantic Meridional Overturning Circulation. *Remote Sensing of Environment. 169,* 150–162.
22. Kilpatrick, K.A., Podestá, G., Walsh, S., Williams, E., Halliwell, V., Szczodrak, M., Brown, O.B., Minnett, P.J., & Evans, R. (2015). A decade of sea surface temperature from MODIS. *Remote Sensing of Environment, 165*, 27-41.
23. Koner, P.K, A.R. Harris, E.M. Maturi, (2015), A Physical Deterministic Inverse Method for Operational Satellite Remote Sensing: An Application for Sea Surface Temperature Retrievals, *IEEE Trans. Geosci. Rem. Sens.*, 53*(11),*5872-5888.
24. Gentemann, C.L., "Three way validation of MODIS and AMSR-E sea surface temperatures", (2014), J. Geophys. Res. Oceans, 118, 2583-2598, doi:10.1002/2013JC009716.
25. Grim, J. A., J. C. Knievel, and E. T. Crosman (2013), Techniques for Using MODIS Data to Remotely Sense Lake Water Surface Temperatures, Journal of Atmospheric and Oceanic Technology, 30(10), 2434-2451, doi:10.1175/JTECH-D-13-00003.1.

Book chapters published:

1. McClain, C. R. and P. J. Minnett, Satellite Radiometry. In Optical Radiometry for Ocean Climate Measurements. Experimental Methods in the Physical Sciences, Vol 47. G.

Zibordi, C. J. Donlon and A. C. Parr, Eds. Academic Press/Elsevier. (ISBN-13: 978-0-12-417011-7), pp 69-72.
2. Minnett, P. J. and D. L. Smith, Postlaunch Calibration and Stability: Thermal Infrared Satellite Radiometers, In Optical Radiometry for Ocean Climate Measurements. Experimental Methods in the Physical Sciences, Vol 47. G. Zibordi, C. J. Donlon and A. C. Parr, Eds. Academic Press/Elsevier. (ISBN-13: 978-0-12-417011-7), pp 201-243.
3. Donlon, C. J., P. J. Minnett, A. Jessup, I. Barton,W. Emery, S. Hook, W. Wimmer, T. J. Nightingale and C. Zappa, Ship-Borne Thermal Infrared Radiometer Systems. In Optical Radiometry for Ocean Climate Measurements. Experimental Methods in the Physical Sciences, Vol 47. G. Zibordi, C. J. Donlon and A. C. Parr, Eds. Academic Press/Elsevier. (ISBN-13: 978-0-12-417011-7), pp 305-404.
4. Corlett, G. K., C. J. Merchant, P. J. Minnett, C. J. Donlon, Assessment of Long-Term Satellite Derived Sea Surface Temperature Records. In Optical Radiometry for Ocean Climate Measurements. Experimental Methods in the Physical Sciences, Vol 47. G. Zibordi, C. J. Donlon and A. C. Parr, Eds. Academic Press/Elsevier. (ISBN-13: 978-0-12-417011-7), pp 639-677.

Introduction

Sea Surface Temperature (SST) is vital to coastal and marine spatial planning, global weather prediction, climate change studies, search and rescue, and ecosystem based management. SST is derived from measurements taken by numerous satellites carrying infrared and microwave radiometers, and measured from moored buoys, drifting buoys, and ships. This project focuses on completing research to improve the quality of the satellite SSTs from existing and new sensors, produce multi-sensor blended gap-free SSTs from US and international datasets, and successfully broaden the use of these products within specifically targeting coastal applications and the Integrated Ocean Observing System (IOOS).

The objectives of this project are to (1) improve and continue generation of satellite SST data and SST analyses in the IOOS DMAC and CF compliant Group for High Resolution Sea Surface Temperature (GHRSST) Data Specification GDS format; (2) distribute and archive these data; and (3) use these improved SST data in applications, many specifically targeted for the Integrated Ocean Observing System (IOOS).

In the full proposal, each task has been assigned to one or more partners. This partnership consists of 28 scientists from industry, academia, and government with wide ranging experience spanning the initial calibration of satellite sensors, development of SST algorithms, assessment of SST uncertainties, production of NRT satellite data, research into data fusion methodologies and the production of blended data sets, research into diurnal warming and the cool skin effect which both affect satellite SST measurements, and applications that utilize SSTs.

FY1-FY5 Tasks

Please note that the NASA tasks are part of a larger NOPP proposal, so while each task below occurs in order, there may be gaps in the numbering. Tasks that have several sub-tasks performed by different groups are repeated with the work for each group as a separate heading.

Task 1.1 Incorporate new GOES calibration into SST processing (Mittaz & Harris). An Algorithm Theoretical Basis Document is continuing to be revised for the recalibration of AVHRR/3 data. The methodology is being imported into a rigorous traceable framework that is being implemented as part of the FIDUCEO project, which is a major European initiative. Dr Mittaz, who has transferred to the University of Reading, is one of the lead investigators for this project, which is far more ambitious in scope than the work proposed in the MISST-2 project. We are maintaining close ties with the FIDUCEO project and anticipate benefitting from the output of their research, which will include recalibrated radiance data and comprehensive traceable uncertainty information.

Task 1.1 Process and distribute AMSR-E, WindSAT, and GMI, AMSR2 in GDS 2.0. (Mears, Gentemann).
All data is being produced in GDS 2.0 format in NRT and distributed through the PO.DAAC. Code has been consolidated and developed with the intention of easily integrating new datasets. Calibration and inter-calibration of specific sensors requires careful consideration of individual sensor characteristics and behavior. RSS retrievals of environmental parameters, including SST, are precisely intercalibrated and produced using a unified code structure. The unified structure has been extended to MISST L3U processing code for all microwave radiometers that are capable of retrieving SST. The code has been adapted to handle WindSat, AMSR2, AMSR-E, TMI and GMI, as well as any additional instruments should they become available. The same code also handles complete dataset reprocessing as well as near-real-time forward processing. This effectively consolidates 10 programs into 1. Version numbers are used as an input parameter, facilitating future upgrades.

Task 1.2 Reprocess GPM GMI (Mears). GMI L3U data has been completely reprocessed and provided to the PO.DAAC. During the submission process, a number of metadata improvements were made, bringing the dataset completely into CF 1.6 compliance. Because the data are now processing using a universal processing system, these metadata improvements also apply to products for the other microwave satellites. We are also making progress on a candidate L2P product and anticipate test files being available before the end of the calendar year.

Task 1.2 Provide recalibrated AVHRR/3 radiances to project and begin incorporating into HRPT processing stream (Mittaz & Harris).
We have developed and tested an (A)ATSR-to-AVHRR brightness temperature matching methodology which will be needed for ascertaining in-orbit calibration parameters. This has included the development of transfer functions to account for spectral response function differences, including the 3.7 micron channel. Matches have been performed against several years' worth of AATSR data for all AVHRR/3 instruments. Despite tight matchup criteria (<5 minutes, <1° view angle, uniformity <0.5 K), this has resulted in datasets of order 10^6 matches for each instrument, albeit primarily at higher latitudes. Recalibrations have successfully been derived for all instruments with the exception of NOAA-15 AVHRR, which is known to be problematic.

An Algorithm Theoretical Basis Document is continuing to be revised for the recalibration of AVHRR/3 data. The methodology is being imported into a rigorous traceable framework that is

being devised as part of the FIDUCEO project, and, as mentioned above, we will participate in end-user assessments and leverage findings and especially datasets from that work as they become available.

Task 1.3 Review current lake temperature algorithms (Crosman)

We have reviewed the strengths, weaknesses and limitations/error sources associated with current lake temperature algorithms and land and cloud masking procedures. This work has been done over the last several years and the results of this survey will be a review paper on lake SST's (over 300 references) that is nearing completion and is expected to be submitted to *Remote Sensing of Environment* by the end of December 2017. Table 1 Summarizes the challenges, and reported problems in the literature of lake SST retrievals, while Fig. 1 summarizes the Observed biases and RMSE reported in the literature. Studies of satellite-derived lake temperature have historically overwhelmingly used split-window algorithms.

Table 1. Summarizes the challenges, and reported problems in the literature of lake SST retrievals

Topic	***Satellite-derived Lake Surface Temperature Problems***	***Suggested Solutions***
Cloud Mask	Cloud-contaminated retrievals widely reported for many lakes	Cloud masks and QC flags specifically designed for lakes needed.
Land Mask	Near-shoreline land contamination of lake SST.	Removal of all pixels within 1-2 pixel width of shoreline or more complex sub-pixel estimations. Satellite visible reflectance-based time-varying shoreline database.
Retrieval Algorithm	SST errors highly variable spatially and temporally between lakes even within the same region. Lack of in situ data and accurate atmospheric temperature and moisture profiles for input into transfer model calculations.	More research comparing the relative improvement of a full radiative transfer model to regional split-window algorithms for lakes. Increased in situ lake temperature monitoring.
Geolocation and Ortho-rectification	Geolocation errors 1-2 pixels widths. In addition, for lakes more than several hundred meters above sea level orthorectification will also be needed to correctly place satellite image.	Verify that satellite data has been geolocated or orthorectified if possible.
Sampling Frequency	In many mid-latitude locales clouds preclude regular satellite observation. Lake temperature, particularly in shallower waters, changes rapidly.	Use a multi-sensor approach to increase sampling frequency. Quantify cloud frequency and develop climatology.
Air-water Interactions and Diurnal Effects	Large air-water temperature differences reduce accuracy of split-window algorithms and also rapidly cool or warm shallow regions of lake, contributing error to a priori lake temperature based on earlier satellite image. Large skin vs. bulk water temperatures are observed.	Develop satellite spatial climatological LWST maps to use as first guess field if certain time has passed. Develop relationships relating skin and bulk lake temperature for biological applications.
Time of Satellite Pass	Many studies found large diurnal variations in LWST. Thus a single-sensor or single time approach may have biases associated with time of day.	Incorporate satellite retrievals during spectrum of times during both day and night to sample diurnal and inter-diurnal variations in LWST.
Processing and QC	Many higher-level SST products produced over lakes are at too coarse of resolution (4 km) to be of use in smaller lakes or near shoreline.	Reprocess higher-level SST product at native satellite pixel resolution.

Validation	Outside of a few lakes, in situ data to rigorously validate satellite-derived lake temperature is lacking	Expand current in situ lake monitoring observations and number of validation (task for next year)
Lake State	High salinity decreases the surface emissivity and low water clarity increases the diurnal warming	Derive monthly maps of current salinity and water clarity to incorporate into sophisticated algorithms.

A lack of *in situ* data (lake buoy temperature and atmospheric profiles) over many lakes results in using split-window coefficients developed for the oceans and that are inappropriate for lakes in many cases. Hulley et al. (2011) and McCallum and Merchant (2012) have used full radiative transfer models forced by atmospheric reanalyses over various lakes to correct lake WST retrievals. However, a lack of in situ validation data over many lakes remains a severe constraint and our recommendation is that these lake-specific algorithms need more tuning and need to be applied consistently to publically-available SST data sets.

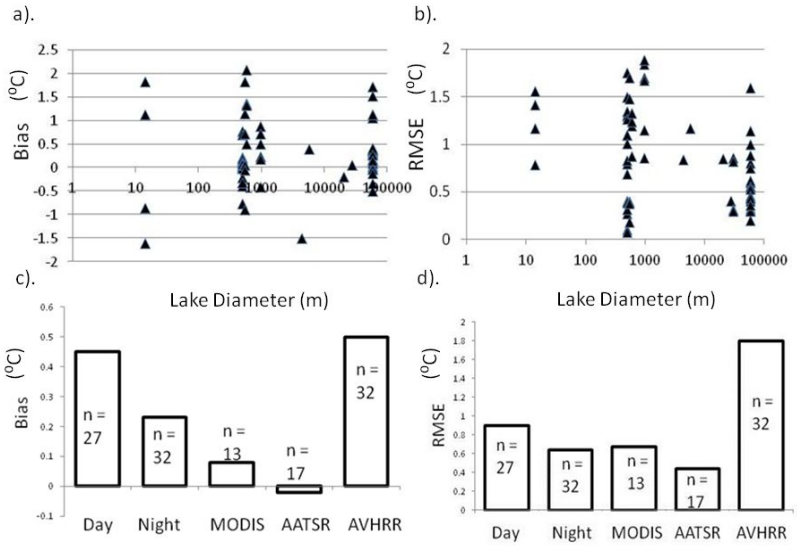

Figure 1. Observed biases (a, c) and RMSE (b, d) reported in lake SST studies between 1980-2013 as a function of lake area (a-b) and satellite platform (c-d).

The results of this work also led to the development of improved land masking, QC, bias-correction, quality-control, temporal compositing, spatial hole filling and spatial smoothing techniques have been presented in the Grim et al. 2013 paper in the *Journal of Atmospheric and Oceanic Technology*.

Task 1.3 Continue evaluation/validation of lake temperature products and recommendations for improvement (Crosman).

1.3a. Improving Lake Temperature for Numerical Weather Prediction

Collaborations between NASA JPL and NOAA/National Weather Service on improving lake temperature retrievals for Numerical Weather Prediction (NWP) was fostered by this project, aided by Inland Waters Working Group meetings during GHRSST. The need for a global, accessible, near-real time lake SST product for NWP was identified and needed steps outlined for the production of this product that will be presented in the review paper. Currently, the

NASA MUR product meets many of the needs for the NWP community. An evaluation of the NASA Multi-scale Ultra-high Resolution (MUR) Sea Surface Temperature products over a several lakes was conducted and presented at the 2017 GHRSST meeting. A subsequent paper evaluating MUR lake SST was published in *Remote Sensing* as outlined in the next section.

Evaluation of NASA MUR Lake SST

This section briefly summarizes the MUR lake SST validation statistics presented in more detail in a paper published in *Remote Sensing*. Daily near real-time MUR lake SST analyses on annual and seasonal time scales have biases below 0.50 K and RMSE below 1.11 K for Lake Michigan and Lake Okeechobee, with the exception of 2014 on Lake Michigan (RMSE 1.62 K) (Table 2 and Fig. 2)

Lake Michigan / Year	Bias (MUR LSWT–In Situ, °C)				Root Mean Squared Error (*RMSE*, °C)			
	Spring (MAM)	Summer (JJA)	Fall (SON)	All Months	Spring (MAM)	Summer (JJA)	Fall (SON)	All Months
2007	−0.07	−0.2	−0.39	−0.24	0.61	1	0.78	0.84
2008	0.43	0.1	−0.41	−0.02	0.59	0.72	0.71	0.69
2009	0.14	−0.43	−0.38	−0.29	0.67	1.4	0.7	1.08
2010	−0.13	−0.56	−0.44	−0.41	0.56	0.76	0.82	0.73
2011	−0.03	−0.47	−0.23	−0.28	0.77	0.87	0.75	0.8
2012	−0.09	−0.29	−0.5	−0.32	0.59	0.65	0.68	0.64
2013	−0.15	−0.27	−0.06	−0.16	0.86	0.68	0.42	0.61
2014	1.92	0.89	−0.07	0.47	2.52	2.19	0.55	1.62
2015	NA	−0.79	−0.33	−0.32	NA	1.03	0.7	0.7
2007–2015	0.25	−0.22	−0.31	−0.2	0.9	1.03	0.67	0.86
Lake Okeechobee (* Statistics Only Calculated for Sample Size n > 6)								
2007	NA *	NA *	NA *	0.27	NA *	NA *	NA *	0.73
2008	NA *	NA *	NA *	0.22	NA *	NA *	NA *	0.99
2009	NA *	NA *	NA *	0.27	NA *	NA *	NA *	0.9
2010	NA *	NA *	NA *	0.1	NA *	NA *	NA *	1.11
2011	NA *	NA *	NA *	0.15	NA *	NA *	NA *	0.9
2012	NA *	NA *	NA *	0.28	NA *	NA *	NA *	1.01
2013	NA *	NA *	NA *	0.25	NA *	NA *	NA *	0.81
2014	NA *	NA *	NA *	0.24	NA *	NA *	NA *	0.8
2007–2014	0.13	−0.13	0.46	0.31	0.69	0.66	1.11	0.91

Table 2. Comparison of MUR versus *in situ* lake SST data.

where diurnal thermoclines impacted the representativeness of the buoy measurements. Over small lakes where MODIS is the only current source of data, large errors in the MUR analyses were noted during periods when cloud cover limits data coverage. However, at this time the MUR lake SST is the only high-resolution near real-time global daily analysis available that resolves thousands of lakes with diameters less than 10 km. Overall, the MUR analyses showed promise for providing real-time analyses of lake SST for lakes larger than a few km in diameter.

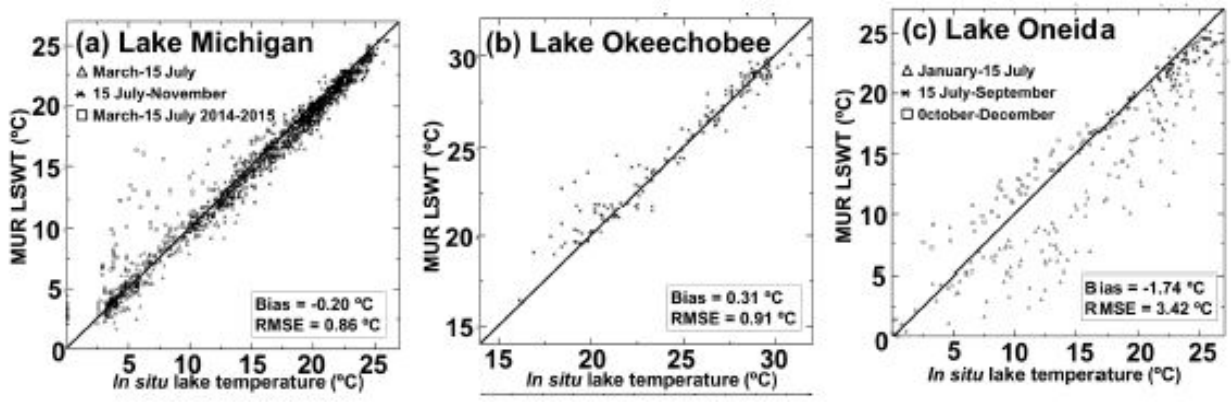

Figure. 2. Scatter plots of MUR LSWT analysis versus *in situ* bulk lake temperature measurements (°C) for period 2007-2015 for (a) Lake Michigan and (b) Lake Oneida. Number of

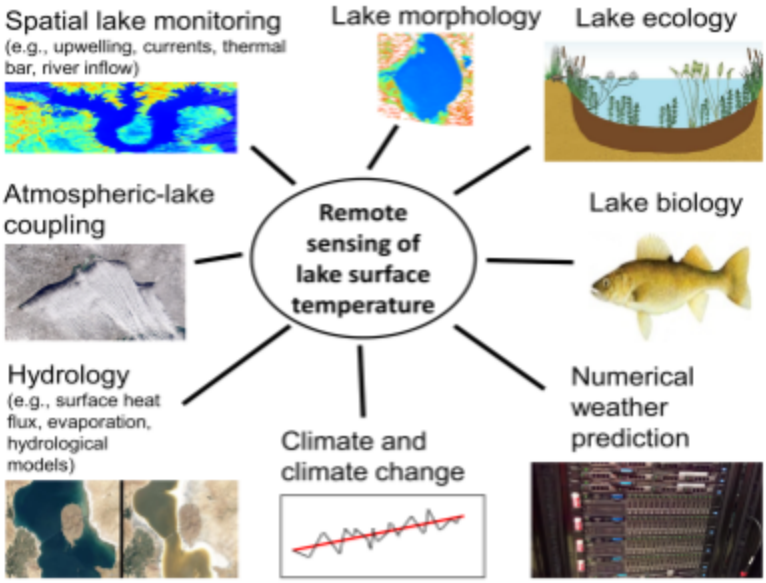

Figure. 3. Key application areas for thermal remote sensing of lake temperature as reviewed in *Crosman et al. 2018*, in preparation

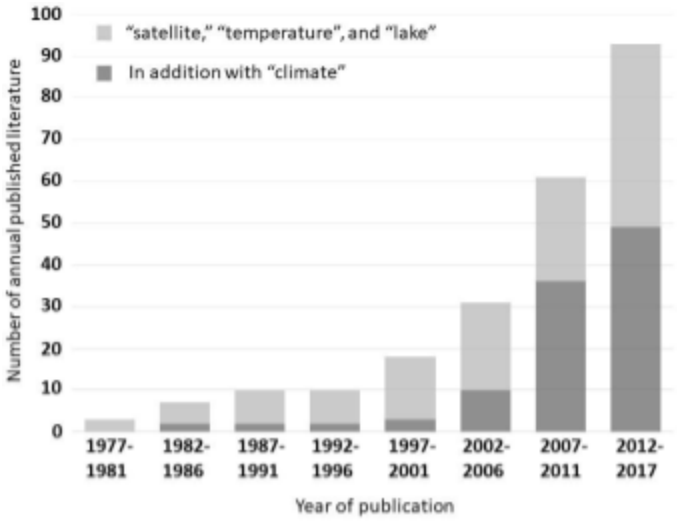

Figure. 4. Number of published literature 1978-2017 listed in the ProQuest Meteorological and Geoastrophysical abstract database containing the terms "satellite," "temperature", and "lake" (light grey bars). The dark grey bars represent the former three terms in addition to the term "climate."

matchups n=1950 for Lake Michigan and n = 281 for Lake Oneida.

1.3b Comprehensive Lake SST Review Paper

A review paper synthesizing over 300 publications on the current state and future needs for lake SST is nearing completion for submission to *Remote Sensing of Environment*. The needs of both the operational numerical weather prediction, limnological, ecological, and climate change communities have been considered (Fig. 3).

The number of publications on remote sensing of lake temperature and climate has increased dramatically in the last decade (Fig. 4), but a lack of vision on the appropriate algorithms to use and how to produce usable climate records with large cloud-induced gaps in coverage of satellite lake temperatures have motivated the review paper.

In the review paper, the evolution of satellite-derived lake temperature over the past 40 years is discussed, with a focus on progress over the last decade and future recommendations. The satellite platforms and algorithms and products available, known sources of error and uncertainty in satellite-derived lake temperature (Fig. 5), applications in numerical weather prediction (Fig. 6), validation of lake SST against in situ observations (Table 3), climate, and hydrological models, as well as future needs for lake SST are discussed.

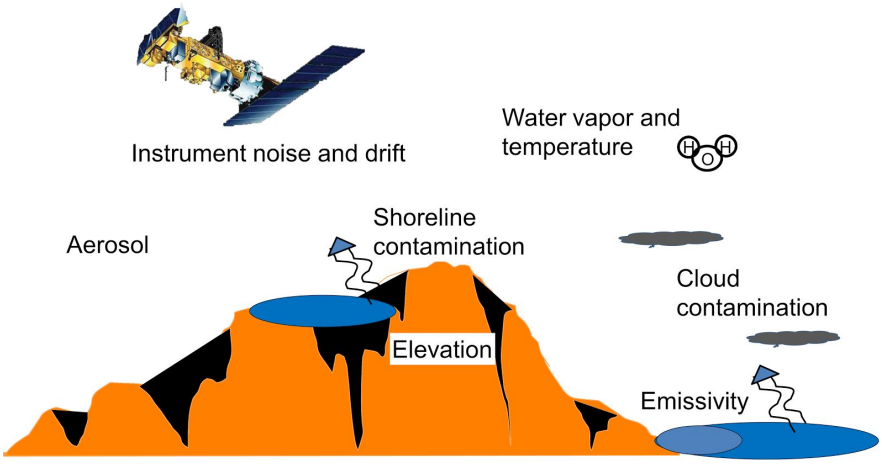

Figure. 5. Sources of error in satellite-derived lake SST.

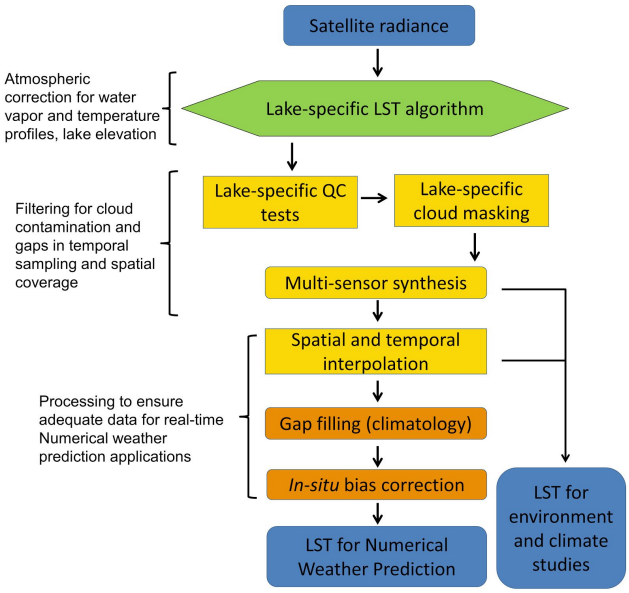

Figure. 6. Proposed processing flow for obtaining improved lake SST for input into numerical weather models.

Table 3. Overview of the *RMSE* reported in the literature for the multitude of lake SST algorithms, instrument platforms, and geographic areas.

RMSE (K) or SD (K)	Instruments (*algorithms*)	Lakes Studied (*references*)
≤ 0.5 K	LANDSAT, ATSR-2, AATSR, MODIS (*IWbST v1.0, Arc-Lake OE, Split window, single channel*)	Lake Iseo (Giardino et al. 2001); Lake Tahoe (*Hook et al. 2003*; *Hulley et al. 2011*); Swedish Lakes (*Reinart and Reinhold 2008*); Salton Sea (*Hulley et al. 2011*); Various global and NA Great Lakes (*MacCallum and Merchant 2012*)
≥ 0.5 ≤ 0.75 K	AVHRR, ATSR-2, AATSR, LANDSAT *(Arc-Lake OE, Split window)*	Lake Malawi (*Wooster et al. 2001*); Lake Biakal (Mogilev and Gnatovsky 2003), Lake Constance (*Thiemann and Schiller 2003*), Various global (*MacCallum and Merchant 2012*) Lake Tahoe (*Hook et al. 2004*) and Salton Sea (*Hulley et al. 2011*). New Zealand lakes (Allan et al. 2016), Arctic lakes (Huang et al. 2015)
≥ 0.75 ≤ 1.0 K	AVHRR, ASTER, MODIS (*Split window, single channel*)	NA Great Lakes (*Li et al. 2001*); Lake Geneva and Constance (*Oesch et al. 2005*); Wisconsin lakes (Becker and Daw 2005)
≥ 1.00 ≤ 1.50 K	AATSR, LANDSAT	Various global (*MacCallum and Merchant 2012*); Argentina reservoir (Lamaro et al. 2013); Lake Geneva (Oesch et al. 2005).
≥ 1.50 K	AVHRR, MODIS (Split window)	Great Slave Lake (*Bussieres and Schertzer 2003*); Great Salt Lake (Crosman and Horel 2009); Quinghai lake (Xiao et al. 2013); NA Great Lakes (Moukomla and Blanken 2016); European alpine lakes (Riffler et al. 2015). Lake Geneva (Oesch et al. 2008). Lake Mond (*Oesch et al. 2005*); Siling Co Lake (Ke and Song 2014)

Task 1.4.1 Refine and validate diurnal maps (Gentemann).
The validation of diurnal models will be extended to include the Zeng and Beljaars (2004) model that has been widely adopted by NWP agencies. We are currently adapting code to run this model. We have been working with the GMAO coupled model to evaluate diurnal warming estimates and improve the models. Two papers have been submitted to Journal of Geophysical Research, Oceans, and are in revision. Gentemann paper: Reviewer comments were received and the paper was revised and re-submitted. Zhang paper: Reviewer comments were received and the paper was revised and re-submitted. A summary of the work is below.

An analysis of the ocean skin Sea Surface Temperature (SST) has been included in the Goddard Earth Observing System (GEOS) - Atmospheric Data Assimilation System (ADAS), Version 5 (GEOS-ADAS). This analysis is based on the GEOS atmospheric general circulation model (AGCM) that simulates near-surface diurnal warming and cool skin effects. Analysis for the skin SST is performed along with the atmospheric state, including Advanced Very High Resolution Radiometer (AVHRR) satellite radiance observations as part of the data assimilation system. One month (September, 2015) of GEOS-ADAS SSTs were compared to collocated satellite Spinning Enhanced Visible and InfraRed Imager (SEVIRI) and Advanced Microwave Scanning Radiometer 2 (AMSR2) SSTs to examine how the GEOS-ADAS diurnal warming compares to the satellite measured warming. The spatial distribution of warming compares well to the satellite observed distributions. Specific diurnal events are analyzed to examine variability within a single day. The dependence of diurnal warming on wind speed, time of day, and daily average insolation is also examined. Overall the magnitude of GEOS-ADAS warming is similar to the warming inferred from satellite retrievals, but several weaknesses in the GEOS-AGCM

simulated diurnal warming are identified and directly related back to specific features in the formulation of the diurnal warming model.

Diurnal warming, wind speeds, and total heat flux, , from four days in September 2015 are shown in Figure 7. In Figure 7a, September 7, AMSR2 SSTs have the largest diurnal warming, then SEVIRI, then the GEOS-ADAS. Both SEVIRI and GEOS-ADAS wind speeds are low for the entire day, with a minimum at 12:00. The GEOS-ADAS underestimates the amount of warming, has a later peak than the satellite data, and then decreases much too rapidly after the peak, disappearing by 18:00; almost always coinciding with when the net heat flux approaches zero. The four panels show diurnal warming at different locations in the Atlantic Ocean and Mozambique Channel. All have low wind speeds during at least part of the day, leading to diurnal warming of the SSTs, however, all of them depict the evolution of the SST differently. The peak amplitude of the GEOS-ADAS warming is equal to or less than the SEVIRI satellite retrieved warming. The satellite retrieved warming shows more variability, likely due to rapidly changing winds, and also always shows more warming in the late afternoon to early evening than the GEOS-ADAS warming. Figure 7 also shows that the 25-km AMSR2 wind speed is less than or approximately equal to the GEOS-ADAS and SEVIRI wind speeds. In Figures 1a and 1c the retrieved AMSR2 wind speed is less than the GEOS-ADAS wind speed and the AMSR2 diurnal warming is larger than in GEOS-ADAS. Whereas in Figures 7b and 7d the AMSR2 wind speed is similar to the GEOS-ADAS and the warming in both of them is also of comparable amplitudes.

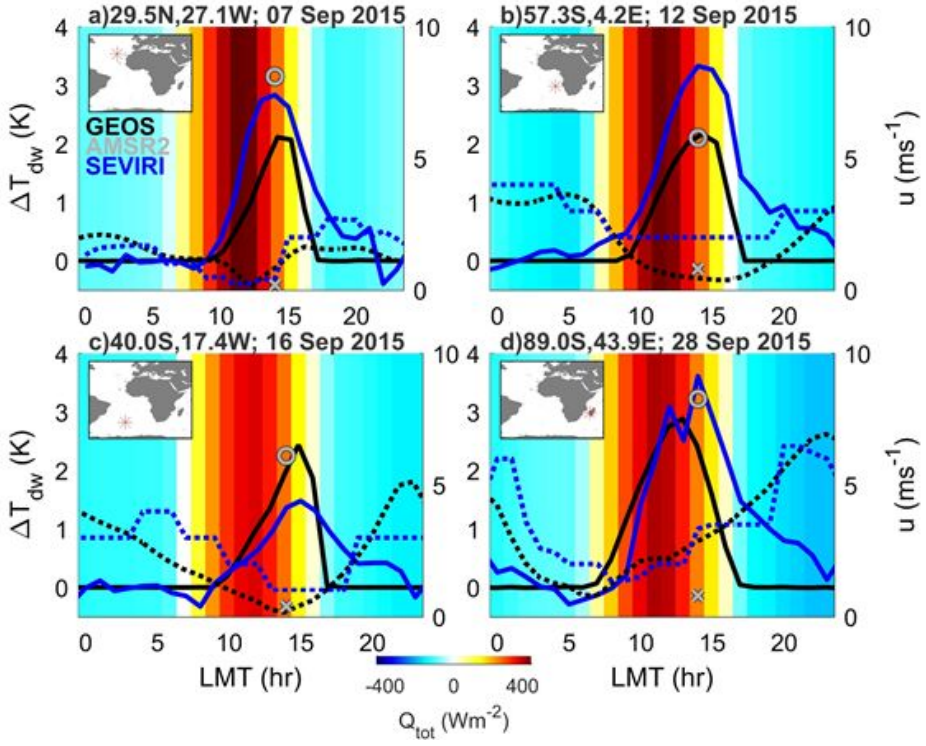

Figure 7. Time series of diurnal warming. SST data is shown by solid lines and 'o', with the axis on the left side of each panel. Wind speed data is shown by dashed lines and 'x', with the axis on the right side of each panel. The date and location is indicated at the top of each panel.

The location of the data time series is also shown in the insert. The GEOS-ADAS data (in black) is always continuous. Days and locations were chosen partly based on availability of SEVIRI data (in blue). AMSR2 data (in gray) is only available near the local equatorial crossing time (LECT) of 1:30 AM/PM. The background colors, Q_{tot} , indicate the total heat flux at the surface (latent, sensible, radiative) as calculated by GEOS-ADAS.

Figures 8 show another analysis method by looking at the data in the same manner as *Gentemann et al.* [2003], where diurnal warming amplitudes were examined as a function of daily average top of atmosphere (TOA) insolation, wind speed, and LMT. A similar analysis was completed for AMSR2 data (not shown). Diurnal warming amplitudes were calculated as described in section 2.3. Ideally, the foundation temperature would be calculated using only the daily minimum temperature, which occurs at approximately 6 AM. The diurnal cycle in cloudiness

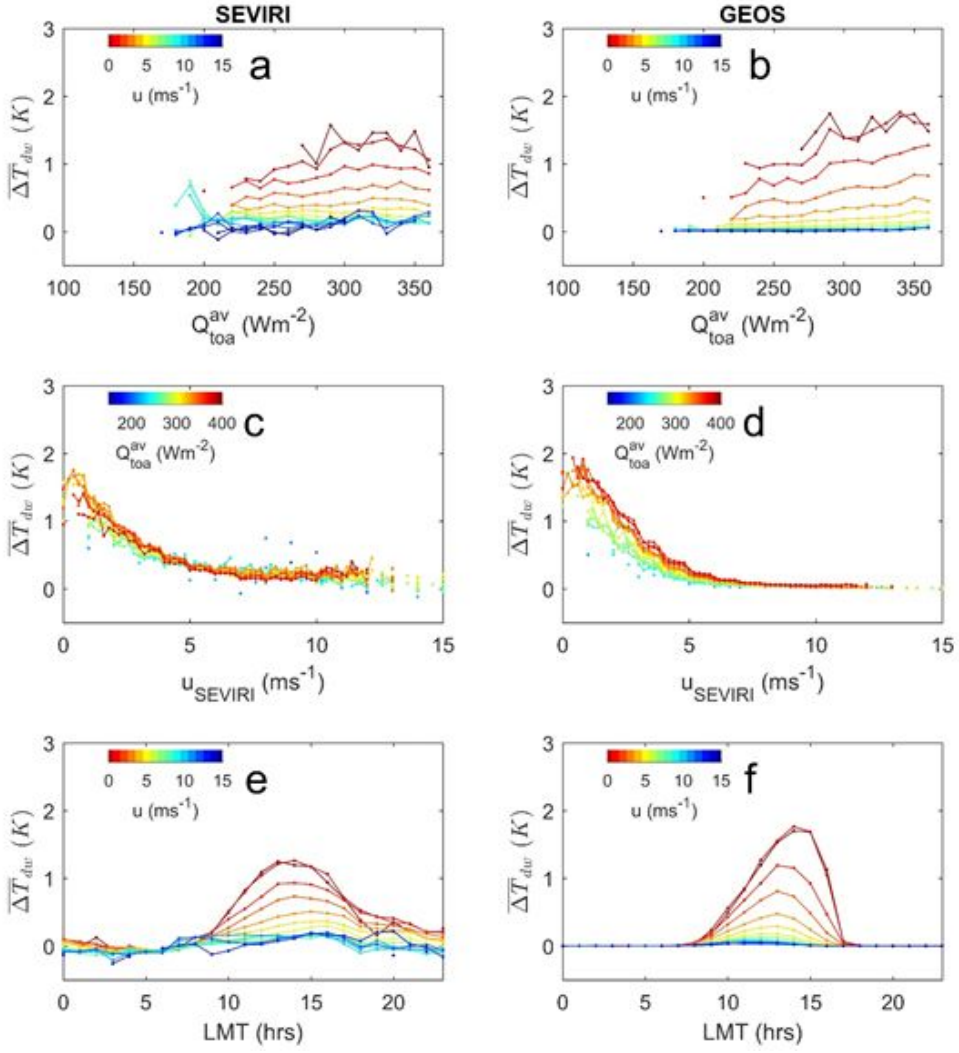

Figure 8. Collocated SEVIRI and GEOS-ADAS diurnal warming as a function daily average TOA insolation (a and b), wind speed (c and d), and Local Mean Time (e and f). The SEVIRI data is in the left column and the GEOS-ADAS diurnal warming in in the right column.

has a peak at sunrise, roughly coincident with the daily minimum in diurnal heating [*Min and Zhang,* 2014]. To avoid large data gaps that would occur when the foundation temperature is 'missing' for a specific location, the nighttime data is averaged over several hours to calculate the foundation temperature. From 3 AM to 6 AM the average diurnal warming is approximately 0 K with little change from 3 AM to 6 AM.

In both Figures 8 and AMSR2 data (not shown) the satellite warming is slightly less than the GEOS-ADAS warming in amplitude. Figures 8a and 8b show diurnal warming increasing linearly as a function of daily insolation. Figures 8c and 8d show an exponential decay in warming with wind speed and Figures 8e and 8f show the daily variability in warming as a function of local mean time. The most striking differences are seen in Figures 8e and 8f where the SEVIRI warming shows a slow decay in diurnal warming in the late afternoon, whereas the GEOS-ADAS warming shows a rapid decay in warming with complete disappearance by 18:00 LMT (as seen in Figure 1). Also, average TOA Figures 8c and 8d show that the GEOS-ADAS warming is larger than the SEVIRI warming at wind speeds below 2 to 3 m s^{-1} (depending on daily average TOA insolation).

Comparisons of AMSR2 and GEOS-ADAS diurnal warming show a problem in the satellite data at high wind speeds, with an unphysical diurnal warming values at low values of insolation. When the analysis is extended for AMSR2 data over the entire year (not collocating with GEOS-ADAS data), this effect disappears, but for September 2015, AMSR2 has a 'cool bias' in the Northern Hemisphere. The diurnal warming in AMSR2 and GEOS-ADAS disappears below approximately 170 Wm^{-2}. There is an exponential decay in warming with wind speed, with very similar amplitudes in warming.

The dependence on wind speed on collocated diurnal warming is more clearly illustrated in Figure 7. The exponential dependence is clear in Figures 5 and 6 and to examine the decay of diurnal warming with wind speed, data were fit to following Equation [1]. Different formulations for this equation were tested and the u^2 in the exponent fit the data best.

$$\overline{\Delta T}_{dw}(Q_{tot}^{av}) = ae^{\frac{u2}{b}} \quad [1]$$

The coefficients *a* and *b* were determined through nonlinear least squares fit of the data shown in Figures 5 and AMSR2 data. Coefficients were determined for daily average insolation values from 250 Wm^{-2} to 360 Wm^{-2} at a local time of 3 PM. Since the magnitude, a, is dependent on the model or data used, only the decay rate, b, is shown in Figure 9. The SEVIRI and AMSR2 wind speed decay rates are very similar, -12.7 and -13.7, respectively. The GEOS-ADAS warming for both collocations with SEVIRI and AMSR2 have the same average decay rate of -6.7. These values yield diurnal warming less than 0.01 K above 5.6 m s^{-1} for GEOS-ADAS and above 7.6 m s^{-1} for the satellite observations. This results indicates that the diurnal model is not mixing heat in the upper layer in the same manner as the retrievals indicate and that the coefficients that control this in the model should be adjusted to obtain more realistic behavior to better match the observational data from satellites.

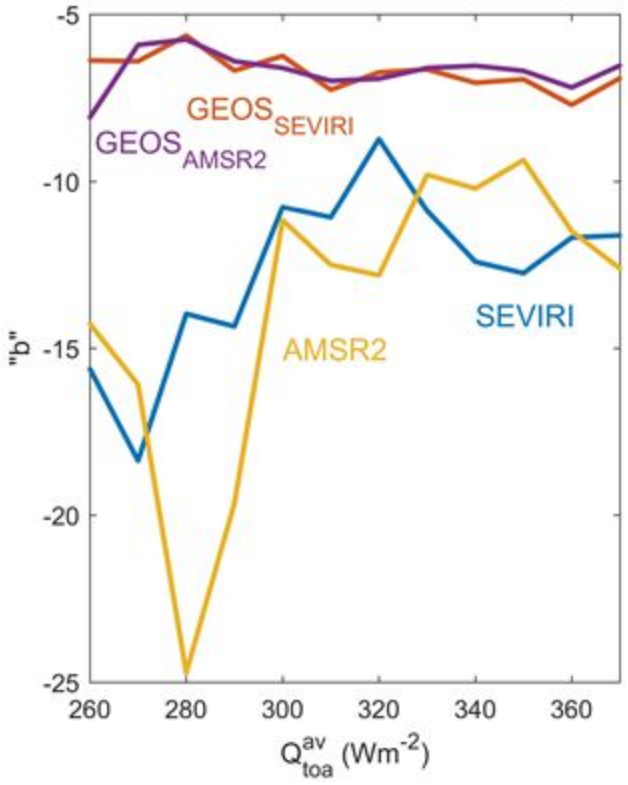

Figure 9. Fit to Equation 1, coefficient b and LMT equal to 15:00.

The diurnal warming in the GEOS-ADAS model isolates the contributions of diurnal warming and cool skin effects allowing the evaluation of them separately. In the satellite observations, while the SEVIRI SSTs are determined from surface radiances, the algorithm used to calculate SSTs was developed using collocated radiance and in situ buoy SST observations. This has the effect of setting the average SEVIRI SST to a bulk temperature. The method that we use to isolate diurnal warming in the SEVIRI SSTs should remove the bulk mean difference and the resultant temperature difference will include components from cool skin effects as well as diurnal warming. For AMSR2, the retrieval is a sub-skin SST, again set to a bulk SST mean through comparisons to buoys. The temperature difference we calculate should be diurnal warming and not have much of a component from the cool skin. All the comparisons that we have done are with the data assimilating GEOS-ADAS diurnal warming calculation, ignoring the cool skin effect. In reality this will only impact the diurnal magnitudes below 2 m s^{-1}, where the skin effect is largest, [*Donlon et al.,* 2002], but the difference should be negligible for the month of data that we have analyzed and we felt that this quantity was the closest to the satellite observations.

Overall the comparisons between SEVIRI, AMSR2, and GEOS-ADAS diurnal warming show encouraging results. The GEOS-ADAS warming has a realistic geographical distribution, matches satellite observed warming through the day, and roughly comparable magnitudes. Teasing out the causes for the differences in retrieved and assimilated warming is a difficult problem and requires analysis from a number of viewpoints. Amplitudes of the diurnal warming

from the satellite data may underestimate the actual surface warming due to algorithm sensitivity and spatial resolution, but these effects shouldn't affect the rate of cooling/warming.

Examination of individual diurnal warming events shows the highly variable nature of diurnal warming. The GEOS-ADAS model matched AMSR2 diurnal magnitudes at 2PM local time when the model wind speeds were close to the satellite derived wind speeds. The SEVIRI warming shows the shape of warming through the day and it was more variable than the assimilated warming and also showed more warming in the late afternoon. These results were also seen in the statistical analysis of warming shown in Figures 5and 6. The GEOS-ADAS' amplitude was close to the diurnal warming seen in AMSR2, but it decayed too quickly with increasing wind speed and decreased much too rapidly in the late afternoon. The amplitude of warming depended strongly on the model wind speed. In all cases, model wind speeds collocated to satellite observations resulted in smaller amplitudes. The most accurate depiction of diurnal warming magnitudes, when looking at them in an average-sense, was when coincident satellite observations of wind speed were available for the validation (Supplemental Figure S1). The SEVIRI amplitudes are lower than GEOS-ADAS, as expected given that the NLSST algorithm sensitivity should result in an underestimation of actual amplitudes. The AMSR2 amplitudes are close to the GEOS-ADAS which should be expected given that they have similar spatial resolutions. In the future, more confidence in the diurnal warming amplitudes estimated from IR SSTs will be possible as data processed using an improved sensitivity algorithm becomes available.

Based on these comparisons, we recommend following modifications to the TBBJ10 model formulation. The Monin-Obukhov similarity model changes form when the stability parameter, changes sign. In the late afternoon, the switch to heat loss causes to change sign and the stability parameter < 0 is in effect. This change results in the unrealistically rapid decay of warming (Supplemental Figure S2). The form of the similarity function was developed based on *Large et al.* [1994] which discusses the dimensionless flux profiles and gives analytic expressions from available data [*Högström*, 1988]. Hence, either the similarity function coefficients should be revisited or the implementation of TBBJ10 model in GEOS-ADAS should be revised; latter approach is being actively investigated within the GEOS- AGCM. In addition to exploring the coefficients, it should be recognized that the TBBJ10 model does not parameterize any heat exchange with the bottom boundary and there is a fixed diurnal warm layer thickness, both of which are unrealistic. Heat exchanges are going to occur at both surface and bottom of diurnal warm layer through mixing and decrease the heat within the layer, and hence require coupling of the diurnal warming model with an OGCM. Also, variability in warm layer depths are well documented and should be considered in future versions of the model [*Delnore*, 1972; *Halpern and Reed*, 1976; *Soloviev and Lukas*, 1997].

Task 1.5 First VIIRS SST uncertainties, including seasonal characteristics; revision of MODIS SST uncertainties; revision of AVHRR SST uncertainties (Minnett).

A significant asymmetry in the discrepancies between S-NPP VIIRS skin SST retrievals and collocated measurements from buoys was identified. (Figure 10). This is very suggestive an imperfect correction for the changing reflectivity of a mirror as a function of incidence angle, the so-called response vs scan angle (rvs) effect. An empirical correction based on the satellite zenith angle has been derived and this removes the asymmetry in the zenith angle dependence of the

errors (Figure 11). The VIIRS data here have been derived with an experimental algorithm that includes additional zenith angle dependences to extend to reduce errors at high satellite zenith angles. Improvements to the algorithms are the subject of continuing research.

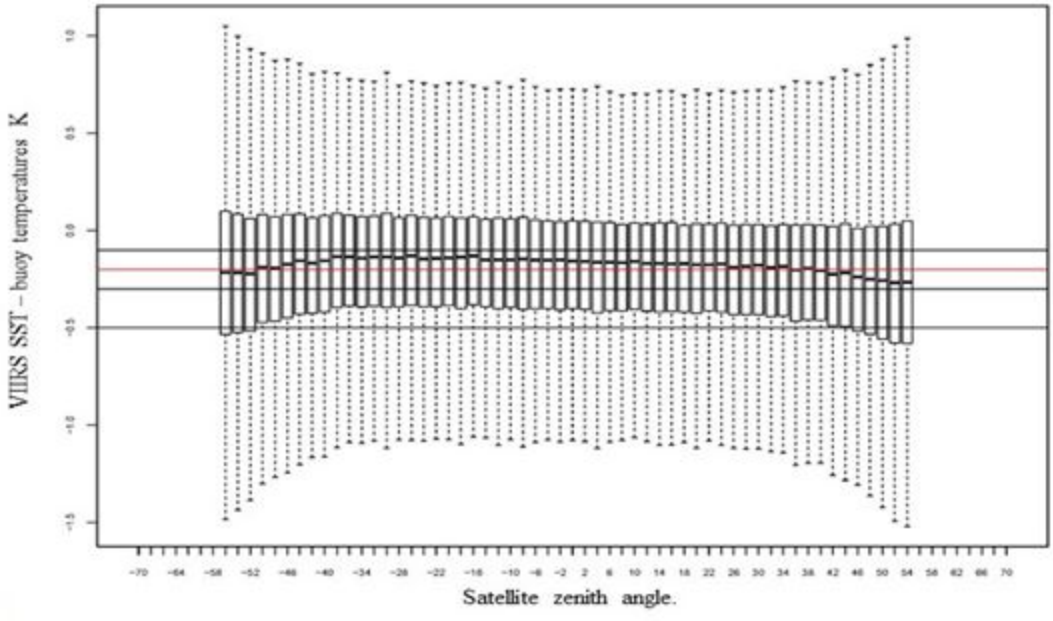

Figure 10, Box-whisker plot of the discrepancies between the VIIRS skin SST and coincident subsurface measurements from buoys. The VIIRS retrievals are based on the split window atmospheric correction algorithms, using measurements from the M15 and M16 bands. The red line indicates the mean thermal skin effect, and ideally the discrepancies should lie on this line. The effects of increasing atmospheric path length, imperfectly corrected by the atmospheric correction algorithm, are expected to produce errors and uncertainties that are symmetrical about nadir.

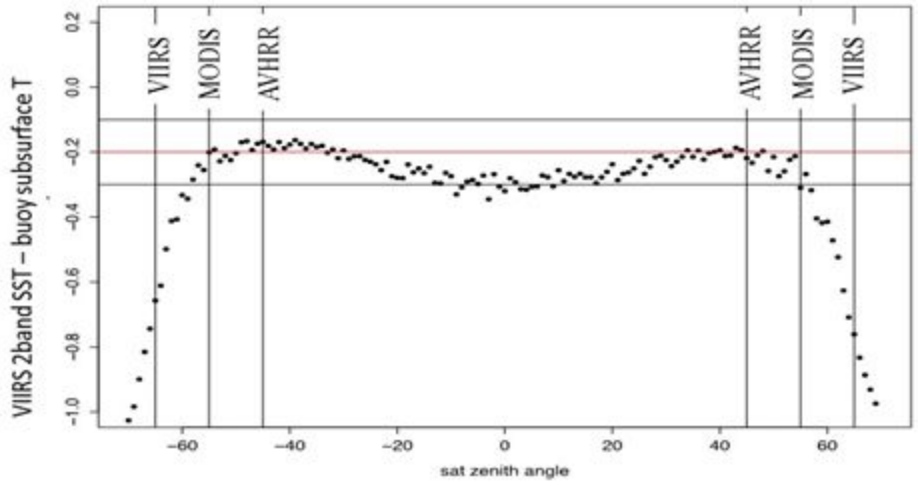

Figure 11, Dependence of VIIRS skin SST discrepancies with in situ measurements as a function of satellite zenith angle. The zenith angle limits for the SST retrievals for AVHRR Pathfinder (45º) and MODIS (55º) are also shown, as is the desired zenith angle limit for the VIIRS retrievals. The asymmetry in the differences with in situ measurements has been reduced.

Structure of SSES

The current form of the SSES's for *Terra* and *Aqua* MODIS and for S-NPP VIIRS are "hypercubes" which are 7-dimensional spaces with cells determined by ranges of parameters that influence the accuracy of the satellite radiometer SST retrievals. The cells are populated by the mean and standard deviations of the values of the matchup data bases for each instrument and corresponding measurements from buoys and ship radiometers. The number of matchups contributing to the statistical variables in each cell is not uniform, and therefore the confidence in the estimates of the means and standard deviations is also variable. We continue to assess the merit of using parametric relationships instead of discrete cell boundaries in the hypercubes.

M-AERI deployments

M-AERIs have been reinstalled on *Celebrity Equinox* and *Allure of the Seas* after refurbishment and recalibration at RSMAS. The M-AERI's have functioned well over much of the period of this project. Monitoring the data acquisition and real-time calibration via satellite internet link indicates the instrument is functioning well. New monitoring software has been developed and installed to improve the efficiency of remote operations. A third M-AERI has been readied for installation on the *Adventure of the Seas* in January 2018 when the ship be undergoing a significant refit. The fourth M-AERI is ready to be deployed on the NOAA Ship *Ronald H Brown* in early 2018.

ISAR deployments

ISARs continue to be deployed on the M/V *Andromeda Leader* that travels between Japan and the USA.

The global statistics of the differences between MODIS SST_{skin} and those from ship-based radiometers are shown in Table 4.

Satellite and Algorithm	***Mean***	***Median***	***St. Deviation***	***Robust St. Dev.***	***Number***
Terra SST Day	*0.082*	*0.080*	*0.567*	*0.409*	*1025*
Terra SST Night	*0.048*	*0.034*	*0.467*	*0.337*	*2454*
Terra SST4 Night	*0.016*	*0.023*	*0.339*	*0.244*	*2467*
Aqua SST Day	*0.105*	*0.107*	*0.666*	*0.480*	*910*
Aqua SST Night	*0.020*	*0.027*	*0.489*	*0.353*	*1752*
Aqua SST4 Night	*-0.010*	*0.016*	*0.396*	*0.285*	*1858*
SST is derived from measurements from MODIS bands 31 and 32 (λ = 11.03 and 12.02 μm) *SST4 is derived from measurements from MODIS bands 20 and 22 (λ = 3.95 and 4.05 μm)*					

Table 4. Statistics of differences between Terra and Aqua MODIS SST_{skin} retrievals and SST_{skin} values from ship radiometers (M-AERI and ISAR). Values are in K.

Task 1.5 Validate MW SSTs to re-develop error estimates (Mears).
The uncertainty in microwave SSTs is computed using a lookup table the describes how the retrieval uncertainty varies as a function of SST and wind speed. These tables were recently rederived using the most recent versions of the SST datasets (V7 from AMSRE, and V8 for TMI, GMI, and AMSR2). The tables are smoothed and extended into regions in SST/Wind Speed parameter space that are measurement-sparse using a non-parametric smooth that minimizes local curvature. These new tables are now available, and are used to find the error estimate for each SST provided to the PO.DAAC

Task 1.5 Cross-comparison of SSES for geostationary SSTs with other SST products, especially MW, to validate success of aerosol correction and derived uncertainties (Harris & Mittaz).
The SSES work using total error calculations for our Modified Total Least Squares physical retrieval method has essentially been completed. Work is continuing on investigating improvements in cloud detection and SST retrievals.

The SSES work using total error calculations for our Modified Total Least Squares physical retrieval method has essentially been completed. Work is continuing on investigating improvements in cloud detection. The new tests are based on utilizing "double-differences" $(T^1_{obs} - T^1_{crtm}) - (T^2_{obs} - T^2_{crtm})$ for various channel combinations. Use of forward-model information has the advantage of "localizing" the test by accounting for regional differences. However, there remains the prospect of erroneous cloud flagging due to errors in the atmospheric profile information used in the forward model. Employing double-differences has the advantage of reducing the impact of such errors in the initial guess NWP profile, since the effects will be similar to first order for the various channels. A form of these tests developed for GOES-Imager has been reported in our recent publication in RSE (Koner *et al.*, 2016). Tests have also been developed on MODIS AQUA data and we find that the data coverage (*i.e.* regions for which good SSTs can be obtained) increases by about a factor 3 *cf.* the conventional cloud mask currently used in the MODIS processing. This work has recently been published in *Remote Sensing* (Koner and Harris, 2016).

Task 1.5 1st version of aerosol correction for geostationary SST (Harris & Mittaz)
The NCEP NGAC aerosol product is about to become operational. We contributed our findings to NCEP's report on the 30-day trial period. Work has continued on optimizing channel selections for inclusion of aerosol total column in the retrieval vector. It should be noted that, while inclusion of aerosol in the forward modeling is beneficial for GOES-Imager SST retrievals, putting total column aerosol (TCA) in the retrieval vector is very difficult using a Total Least Squares method, which requires at least N+1 pieces of information, *i.e.* 4 or more channels. While the GOES-Imager has 4 channels in the thermal IR, the water vapor channel is only sensitive to upper level moisture, thus the information is only weakly connected to the total column H_2O that is in the retrieval vector, while it has essentially no sensitivity to SST or aerosol. Thus, our studies utilize MODIS data for now, in preparation for the next generation of geostationary imagers (primarily GOES-R Advanced Baseline Imager). Figure 12 shows the Truncated Total Least Squares (TTLS) retrieval differences *cf.* buoy SSTs for various MODIS thermal IR channel combinations. Because the numbers actually approach the expected error in

buoy data (0.23 K - O'Carroll *et al.*, 2008) it is likely that the actual TTLS SST errors are better than this. It can be seen that there are a number of algorithms which perform thereabouts equally well, with what are exceptional results in terms of accuracy, especially the limitations of the *in situ* data. While it might be expected that adding channels always leads to better results, the fidelity of the fast forward model needs to be considered. Systematic mismatches between observed and modeled channel brightness temperatures will erroneously inflate the regularization strength with concomitant reduction in information content. Future improvements in fast forward modeling (possibly from better channel/instrument characterization) should lead to better performance for such channels. In particular, the inclusion of channel 12 seems to degrade results *cf.* other combinations.

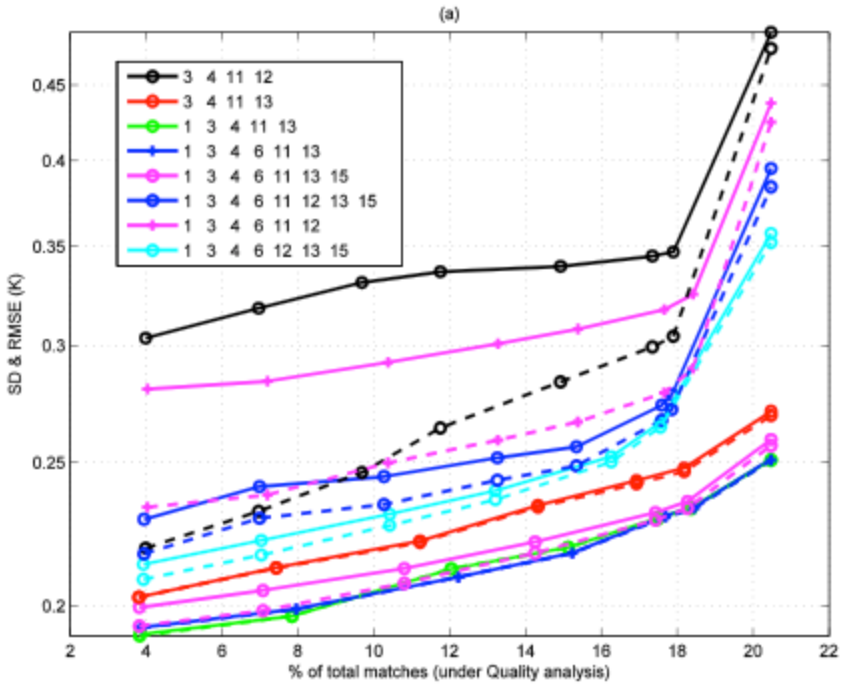

Figure 12. RMSE (solid lines) and Std. Dev. (dashed lines) for TTLS-based retrieval of [SST, TCWV, TCA] for various MODIS channel combinations indicated in the figure key. Note the range of the y-axis is somewhat logarithmic and extends to a maximum value of <0.5 K.

The effect of including TCA in the retrieval vector on the algorithm sensitivity can be seen in Figure 13. It is notable that the improvement of retrieval accuracy over the 2-parameter MTLS comes with improved sensitivity to SST. This is primarily due to the reduced regularization strength, which results from the better "fit" of the Jacobian components to the brightness temperature residuals (MODIS - CRTM) made possible by the inclusion of aerosol in the state vector. Thus, the fraction of brightness temperature differences due to aerosol that were previously contributing to SST and water vapor are now correctly being attributed to the aerosol component of the signal. As a consequence, not only are the SSTs more accurate (essentially "flat-lining" at ~0.2 K due to the accuracy of the *in situ* data), but the information gain with respect to the initial guess accuracy is improved. This is evident by the greater separation

between the TTLS retrieval and initial guess *cf.* the previous (MTLS) version. Put another way, the redistribution of the initial guess error to generally higher values while reducing retrieval error is highly desirable, since it implies the new 3-parameter TTLS retrieval is less dependent on an accurate initial guess SST to get a good result.

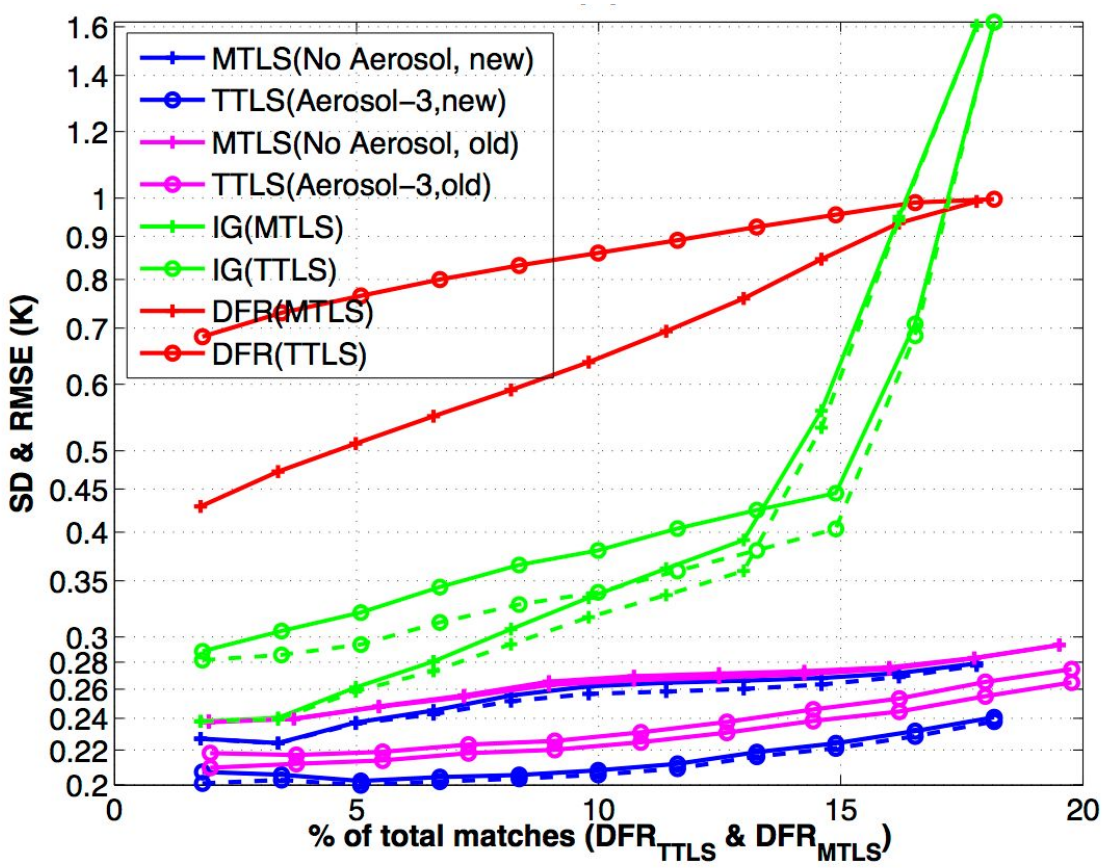

Figure 13. RMSE (solid lines) and Std. Dev. (dashed lines) for MTLS-based retrieval [SST, TCWV] "+" and TTLS-based retrieval [SST, TCWV, TCA] "□" as indicated in the figure key. The initial guess accuracy (*i.e.* the magnitude of adjustment required to get an accurate retrieval) is shown in green. The sensitivity to SST is shown in red for the MTLS and TTLS. It can be seen that the 3-parameter TTLS retrieval has lower noise and higher sensitivity, and is above 0.9 when the required SST adjustment is greater than 0.4 K.

SLSTR Validation

The recently-launched Sentinel-3 platform carries the Sea and Land Surface Temperature Radiometer (SLSTR), which is the next-generation version of the Along-Track Scanning Radiometer series of instruments. These are the only SST-capable imaging radiometers with climate monitoring accuracy as the primary driver in their design. We have conducted validation of both the initial and revised versions of the SLSTR SST products against high-quality ARGO data. The advantages of ARGO are good geographic distribution outside the cloud-free ocean and shallow seas, and very high calibration accuracy *cf.* traditional drifting buoy sensors. The main disadvantage is that the shallowest measurements are usually several meters below the

surface. Thus, we have used our turbulence-based diurnal warming model to identify and adjust cases where there are thermal gradients in the upper ocean, in order to obtain a more representative temperature for comparison with the SLSTR SST retrieval. In keeping with the previous ATSR instruments, the retrieval algorithms are based on radiative transfer modeling rather than direct regression against *in situ*, in order to preserve independence and also enable dynamic quantification of regional biases. Thus the validation against *in situ* represents a genuinely independent test of product quality. Figure 14 shows the the dependence of nighttime SLSTR retrievals using the 2-channel nadir-view (N2, left panel) and 3-channel dual-view (D3, right panel) against total column water vapor. While the D3 is expected to be the more accurate algorithm, the existence of a marked dependency on water vapor in the N2 is indicative of a radiative transfer modeling error, which is currently being investigated by the algorithm development team. *N.B.* This is only one of several findings we presented at the Sentinel-3 Validation Team Meeting held at ESA-ESRIN in February 2017.

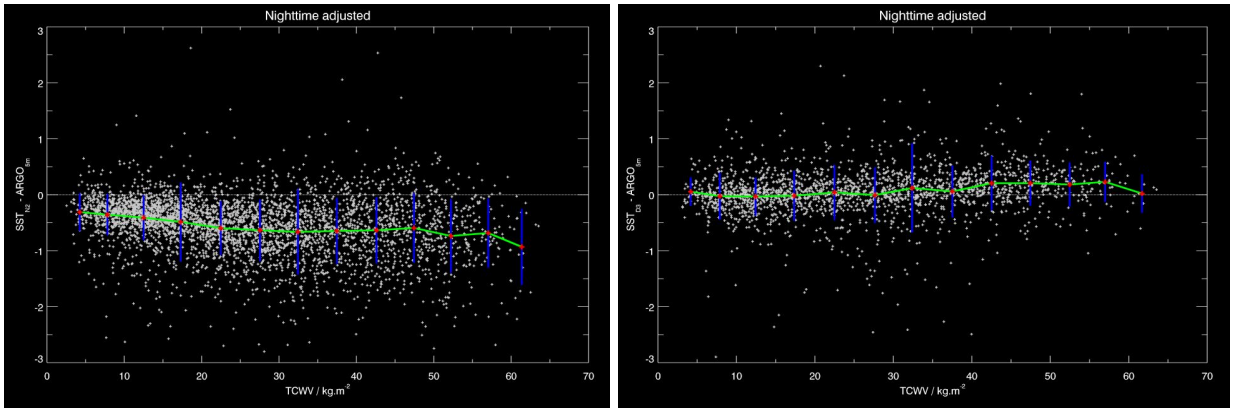

Figure 14. Difference between nighttime SLSTR SST retrievals (adjusted to ARGO depth) and ARGO temperatures. Left panel shows results for the nadir-only 2-channel SST retrieval, while the right panel shows the dual-view 3-channel SST retrieval

An analysis of the first year of Sentinel-3 SLSTR SST data has been undertaken, again using ARGO data as a reference and our turbulence-closure diurnal warming model, and the results were presented at the 2017 Eumetsat meeting in October 2017. Since the cloud detection and SST retrieval algorithms have been through several iterations during this time, there is significant work required to make the results as consistent as possible. It can be seen from Figure 15 that changes to the retrieval coefficients have altered the water vapor dependence of the N2 algorithm and, to a lesser extent, the D3 algorithm, but not removed it completely. Thus, it seems that not all the issues have been resolved. The Bayesian cloud detection is yet to be implemented in the Sentinel-3 SLSTR operational data stream, which is another key step, since the current cloud detection, although somewhat improved, still shows significant cloud leakage, along with a marked asymmetry in day/night results, suggesting substantial false-flagging in the daytime. Bringing the SLSTR data into line with expected capabilities is important to safeguard the integrity of the SST record for many oceanography and climate applications, since it is the only thermal infrared SST sensor with inherent robustness to volcanic aerosol events (the recent activity of Mt Agung is a reminder of this risk).

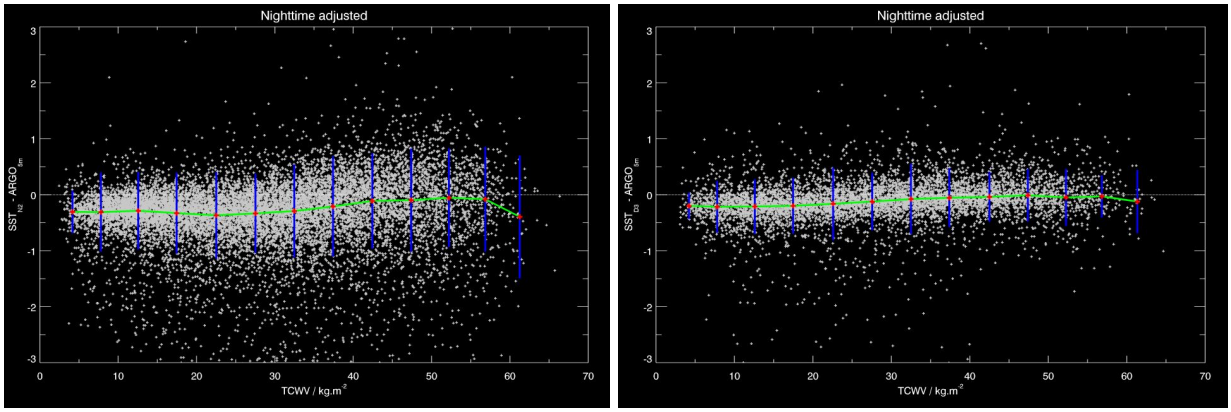

Figure 15. As for Figure 14 but with revised SST retrieval coefficients, and a year's worth of data, for the N2 algorithm (left panel) and D3 algorithm (right panel). The behavior of the N2 algorithm in particular is different from the previous version, but water vapor dependence is still evident. Note also that residual cloud contamination persists in the revised data, as evidenced by cold outliers in the N2 retrieval.

Diurnal modeling enhancements

The turbulence model used to estimate upper ocean thermal structure continues to be a valuable tool for our work, both in validation (see above) and also in assimilating observations from different platforms at various times of the day into a single SST analysis. One of the most challenging issues has been in finding a configuration that works well in all geographical locations. We have recently developed a new parameterization that is now being tested in combination with a factor for unmodeled wind gustiness. Figure 16 shows a comparison of the distribution of diurnal amplitudes at 1400 UTC for the month of August 2015 for the model prediction and SEVIRI observations. The left-hand panel shows the results for the previous model configuration, while the right-hand panel shows the new configuration with a modest gustiness factor.

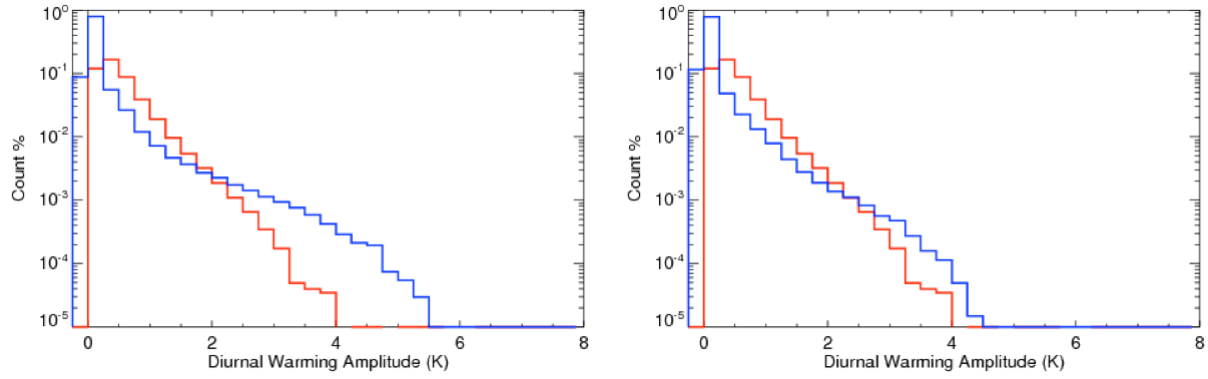

Figure 16. Distributions of diurnal warming amplitude at 1400 UTC during August 2015 as predicted by turbulence model (blue) and observed by SEVIRI (red). Left panel shows the old model configuration, while the right panel shows model results for incorporating a new parameterization and modest gustiness factor. *N.B.* SEVIRI results are unchanged between the 2 plots.

At RSMAS, a project to understand better the effects of tidal flow over complex topography is nearing completion. The objective to to elucidate the effects of vertical mixing over the Great Barrier Reef in controlling the amplitudes of diurnal heating over the corals.

Reprocessing of geostationary data using physical retrieval

The recent success of our MTLS physical retrieval methodology (*e.g.* Koner *et al*., 2015) has led to requests to reprocess the geostationary record. This has required an extensive effort to collect radiance data (~150 TB) from the archives (CLASS, Eumetsat and Australian BoM), along with

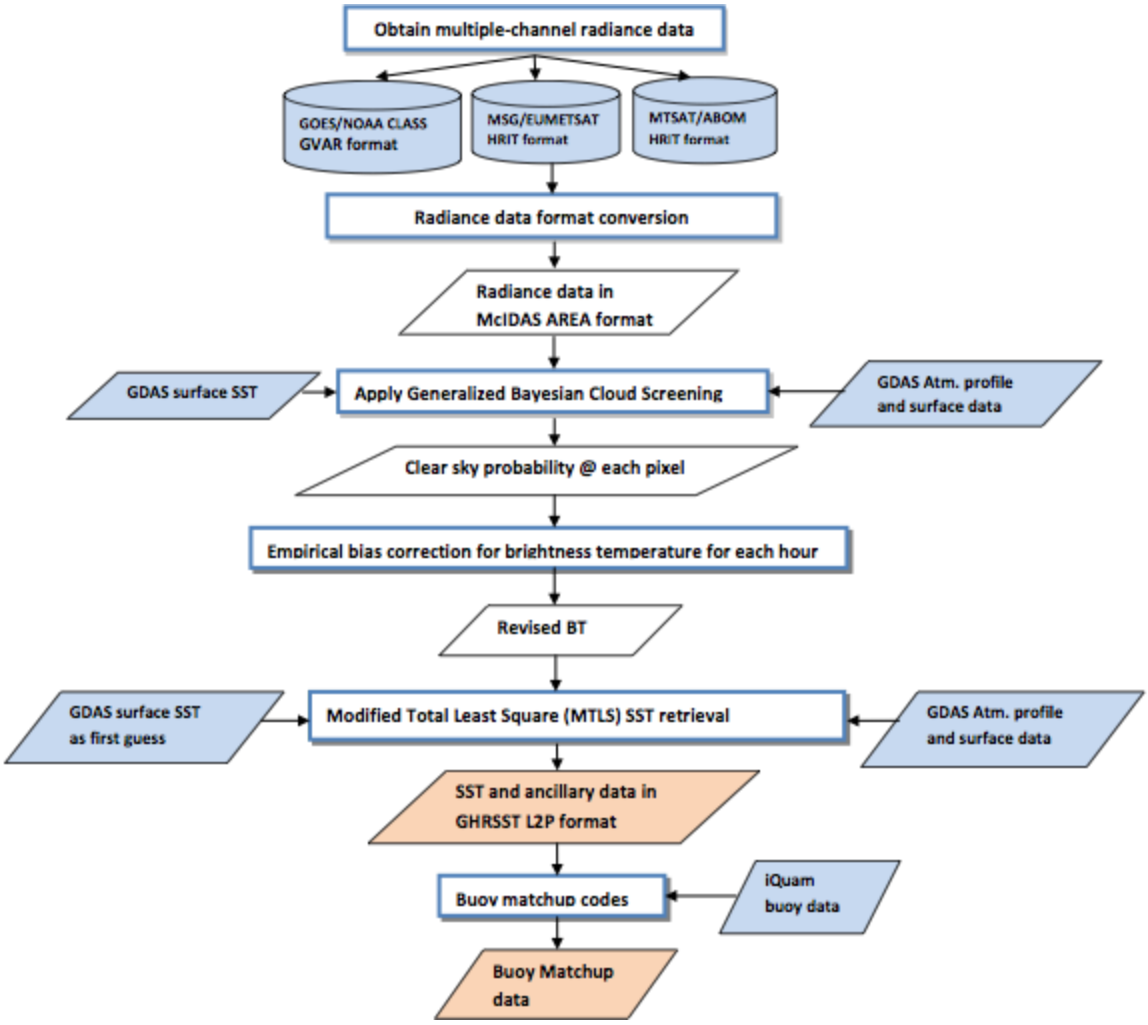

Figure 17. Flowchart of the reprocessing procedures. The input data are shown with the light blue background, and the output data are shown with the light orange background.

associated ancillary data (chiefly NCEP NWP surface and upper air analyses). An overview of the processing flow is shown in Figure 17. The reprocessing has resulted in dramatic improvements in both accuracy (noise) and stability of the SST products compared with the previous operational versions. Figure 18 shows the results for the three platforms that have been operational in the GOES-W location (subsatellite point 135°W) since 2002. Note that the MTLS retrieval was implemented towards the end of 2013, thus the results from that point onward are identical. A paper on this geo-SST reprocessing effort has been submitted to Remote Sensing of

Environment (Zhu *et al.*, 2017). This work was shown as a poster presentation at the 18th GHRSST Science Team Meeting. The record is now being extended back to end-1994, corresponding to the launch of GOES-8, which was the first 3-axis stabilized operational geostationary sensor that carried the properly SST-capable 10-bit resolution GOES-Imager on-board a 3-axis stabilized platform. (The latter feature allowed the imager scan pattern to be much more directed to the Earth, thus greatly improving signal-to-noise *cf.* the previous spin-scan mounted VISSR instrument, which could only spend a small fraction of its time pointing at the target.) This unique dataset will be a powerful tool for studying diurnal cycles in SST, and for providing better daily coverage than available from polar-orbiting sensors alone. The data have already been used in a reprocessing of the NOAA 5-km Geo-Polar Blended SST analysis that is the foundation of a new climatological baseline for the development of enhanced NOAA Coral Reef Watch ecological monitoring products.

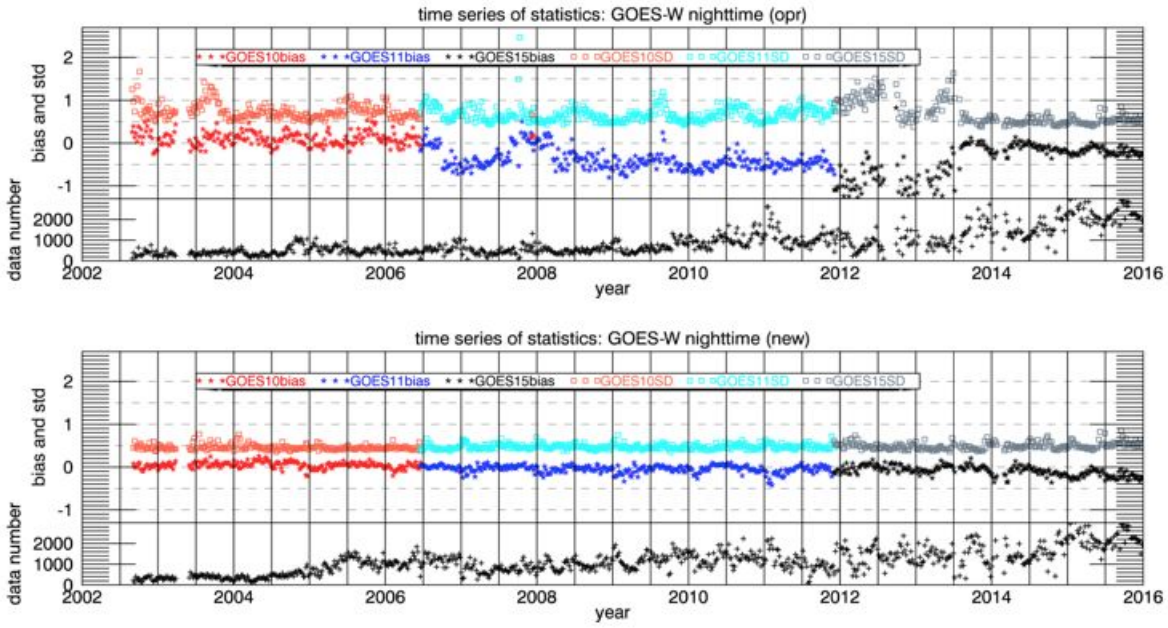

Figure 18. Time series of bias and standard deviation of the operational (top) and reprocessed (bottom) SST against buoy for the entire time period of September 2002 to December 2015 for GOES-W night time. Each point in the bias and SD time series is calculated using hourly matches in a 5-day time window. The lower panel in each plot shows the number of matches in each 5-day window

Task 2.3 Attend IOOS RA annual meeting to present MISST SST datasets (Gentemann). Outreach and coordination via email was completed during the project. Mike Chin has created a MUR anomaly at the request of an IOOS RA.